Journal of Molecular Graphics and Modelling 120 (2023) 108419

Contents lists available at ScienceDirect

Journal of Molecular Graphics and Modelling

journal homepage: www.elsevier.com/locate/jmgm

Theoretical studies on the reaction mechanisms of the oxidation of tetramethylethylene using MO_3Cl (M=Mn, Tc and Re)

Emmanuel Adu Fosu [a], Collins Obuah [a,c,*], Louis Hamenu [a], Albert Aniagyei [b], Anita Oppong [a], Michael Kojo Ainooson [a,c], Alfred Muller [c]

[a] Department of Chemistry, University of Ghana, Legon, Ghana
[b] School of Basic and Biomedical Sciences, University of Health and Allied Sciences. Ho, Ghana
[c] Department of Chemical Sciences, University of Johannesburg, Auckland Park Kingsway Campus, Auckland Park, 2006, Johannesburg, South Africa

ARTICLE INFO

Keywords:
Quantum methods
Reaction mechanisms
Oxidation
Diols
Epoxides

ABSTRACT

A theoretical study on the reaction mechanisms of the addition of transition metal oxo complexes of the type MO_3Cl (M = Mn, Tc, and Re) to tetramethylethylene (TME) is presented. Theoretical calculations using B3LYP/LACVP* and M06/LACVP* (LACVP* is a combination of the 6-31G(d) basis set along with LANL2DZ pseudo-potentials on the metallic centres) were performed and the results are discussed within the framework of reaction energetics. The nature of the stability of the reaction mechanisms was equivalent for both theories. However, the M06/LACVP* simulations generally had slightly lower energies and shorter bond lengths compared to the B3LYP/LACVP* computations.

Furthermore, it was observed that the reaction does not proceed *via* the stepwise reaction mechanism due to kinetic and thermodynamic instabilities. Epoxidation was also found to occur *via* the [2 + 2] concerted reaction mechanism for the MO_3Cl (M = Tc and Re) whereas the permanganyl chloride complex epoxidizes TME *via* the [2 + 1] concerted reaction mechanism on the singlet potential energy surface (PES). Dioxylation was observed to proceed *via* the [3 + 2] route for the addition of MO_3Cl (M = Tc and Re) and TME. Results indicate that all reaction surfaces were unselective except for the permanganyl chloride catalyzed surface which leads to the formation of epoxides exclusively.

Changes in temperatures from 298.15 K to 373.15 K, resulted in kinetically and thermodynamically unstable reaction pathways as the activation and reaction energies increased generally. On the singlet PES, the rate constant calculations showed that the [3 + 2] catalyzed surface reaction mechanism leading to dioxylation was faster than the [2 + 2] mechanism in cases where plausible.

Theoretical values from the global reactivity parameters, namely the chemical hardness, chemical potential, electrophilic and nucleophilic indices, are in good correlation with the DFT activation and reaction energies at both levels of theories. Thus, as the electrophilic nature of the metal decreases from Mn to Re, so do the activation and reaction energies increase from Mn to Re, indicating that the higher the electrophilicity of the metal centre, the more spontaneous the oxidation reaction.

1. Introduction

Nowadays, the use of quantum methods such as density functional theory (DFT) and *Ab Initio* techniques have become essential for investigating the fascinating molecular mechanisms and structural challenges posed by chemical processes.

The Kohn–Sham density functional theory (KS-DFT) has been widely utilized for several applications in chemistry, condensed-matter physics, and materials science, but the accuracy of KS-DFT depends on the approximations made to the exchange-correlation functional [1,2]. The M06 and B3LYP models, which are hybrid functionals, have been widely used due to their broad applicability in studying chemical systems. The B3LYP functional, a Hartree–Fock DFT model [3,4] is made up of the exchange-correlation energy from the local spin-density approximation (LSDA) model, 20% of the difference between the Hartree–Fock exchange energy and the LSDA exchange energy, 72% of the Becke

* Corresponding author. Department of Chemistry, University of Ghana, Legon, Ghana.
E-mail address: cobuah@ug.edu.gh (C. Obuah).

https://doi.org/10.1016/j.jmgm.2023.108419
Received 9 November 2022; Received in revised form 3 January 2023; Accepted 17 January 2023
Available online 25 January 2023

exchange potential, 81% of the Lee-Yang–Parr correlation potential [5] and 19% of the Vosko–Wilk–Nusair potential [6]. The B3LYP functional is one of the most widely used exchange-correlation functionals in organometallic chemistry. Furthermore, the M06 functional [7] is a global hybrid meta-generalized gradient approximation (meta-GGA) with 27% of Hartree–Fock exchange energy, leading to a well-balanced functional for overall good performance for studying chemical systems.

Over recent years, the M06 functional has thus been recommended for application in organometallic chemistry [7–9]. To date, the M06 and B3LYP models are the two most popular DFT tools used in studying organometallic transformations [7,9,10]. M06 is currently the first choice of functional for energy calculations of transition metal systems, followed by B3LYP, DFT-D3, and M06L [9] for the computational studies on synthetically relevant homogeneous organometallic catalysis.

Modern-day chemistry demands researchers to design and develop new catalysts for chemical reactions to help achieve high selectivity and efficiency [11,12]. Oxidation reactions remain one of the most efficient methods in the synthetic tool kits for chemists due to the widespread applications of oxidized substrates in the chemical industry. Debates surrounding the mechanistic details of the formation of vicinal diols from olefinic substrates catalyzed by osmium tetroxide, a typical and well-known oxidation reaction have been resolved by several quantum chemical studies which predicted the [3 + 2] route to be both kinetically and thermodynamically stable than the [2 + 2] pathway [11,13,14, 14–19]. The use of osmium and its oxo complexes as catalysts is very useful in chemical synthesis. However, factors such as toxicity, its expensive nature, scarcity, and volatility demerit its use and urge scientists to explore other options.

In recent years, theoretical and experimental procedures have focused on rationalizing theories around the electronic and structural nature of group VII B elements [17,19–21]. Group VII B transition metal elements (Mn, Tc, and Re) and their oxo complexes continue to be of great asset to chemists due to their ability to oxidize olefinic substrates [12,22,23]. Hence, that was why the oxo complexes of Mn, Tc, and Re were employed in this study. Although several theoretical and experimental works on the reaction of ethylene with metal oxo complexes are known, the same cannot be said for the reactions involving substituted ethylene.

Some of the few theoretical works on the oxidation of tetramethylethylene (TME) by transition metal oxo complexes were done by Wistuba et al. [24] and Aniagyei et al. [25]. Wistuba et al. [24] studied the oxidation of ethylene mediated by permanganyl chloride by theoretical and experimental means. Per the DFT results, Wistuba et al. [24] predicted that the [3 + 2] addition of tetramethylethylene (TME) to the MnO_2 moiety of MnO_3Cl is thermodynamically favoured over the [2 + 1] mechanistic route. In addition, Wistuba et al. [24] experimentally investigated the TME/MnO_3Cl system through matrix-isolation techniques and concluded that the selective formation of the epoxidation product [$ClO_2Mn\{O[C(CH_3)_2]_2\}$] was observed.

Aniagyei et al. [25] on the other hand explored the singlet and triplet PESs for the same reaction only theoretically at 298.15 K and 0.00001 atm at the B3LYP/LACVP* level of theory. The results also predicted that the pathway leading to the formation of the five-membered dioxylate intermediate *via* the concerted [3 + 2] addition was kinetically and thermodynamically stable over the three other possible pathways, thus, the [2 + 2] addition via the transient metallaoxetane intermediate, epoxidation, and hydrogen transfer pathways. Aniagyei et al. [25] also noted that kinetically, both the stepwise and the concerted [2 + 1] addition pathways leading to the epoxide precursors were very competitive with an activation barrier difference of lesser than 0.7 kcal/mol.

This work, therefore, employs the hybrid functional DFT models, B3LYP and M06 in conjunction with the basis set LACVP* to extend the works by Wistuba et al. [24] and Aniagyei et al. [25] by investigating all the concerted and stepwise mechanistic channels resulting from the addition of MO_3Cl (M = Mn, Tc, and Re) across the olefinic bonds of TME. Results from this study will be very useful for experimentalists in the design and use of group 7b oxo complexes as catalysts for the selective oxidation of TME.

1.1. Computational details

In this theoretical study, the DFT/HF hybrid functional model [5,6, 26] B3LYP, and M06 were employed as implemented in Spartan'16 V.2.0.7 [27] in conjunction with the basis set of LANL2DZ for the transition metals (Mn, Tc, and Re), and the split valence double-ξ (DZ) [28] 6-31G (d) for other atoms (C, H, O, Cl).

The MO_3Cl (M = Mn, Tc, and Re) and TME systems on the singlet and triplet surfaces were computed as neutral structures. The Spartan's graphical model builder was used in modeling the molecular systems of the starting geometries. The modeled geometries were minimized interactively using the Sybyl force field [29]. Full optimization of all stationary points on the PES was done without any symmetry constraints. The nature of the stationary points was verified by performing a normal mode analysis. All molecular structures on the minima or equilibrium geometries were characterized by the absence of imaginary frequencies corresponding to any mode of vibration in the system. The saddle point structures were located by a series of constrained geometry optimizations in which the forming – and breaking – of bonds were fixed at various lengths while the remaining internal coordinates were optimized. The approximate stationary points located from such a procedure were then fully optimized using the standard transition state optimization procedure in Spartan [27]. All first-order saddle points were shown to have a Hessian matrix with a single negative eigenvalue, characterized by an imaginary vibrational frequency along the reaction pathway. In cases where no molecular structures could be optimized from the saddle point, a PES scan was performed to verify this observation. This study reports energies in Gibbs free energy values at a temperature of 298.15 K and pressure of 1 atm using unscaled frequencies unless otherwise noted. The imaginary frequencies corresponding to the vibrations along the reaction pathway for each transient structure can be found in Tables S1–S3. Also, the cartesian coordinates for all optimized stationary points can be found in Data S1–S2.

2. Results and discussion

2.1. Reaction of ReO_3Cl with TME

Fig. 1a–e represent the relative Gibbs free energy profile, optimized transition state structures located on the singlet PES and a graphical representation of the interaction between the frontier molecular orbitals of the reactants respectively.

The ground state DFT/B3LYP and DFT/M06 optimization of the ReO_3Cl molecular system on both singlet and triplet PES yielded a tetrahedron geometry with C_1 symmetry. This indicates the absence of all symmetry elements except the identity operation, thus the rhenium oxo complex has no symmetry. On the singlet PES, the DFT/B3LYP computed Re=O and Re-Cl bond lengths of the ReO_3Cl optimized complex were found to be 1.704 Å and 2.265 Å respectively whereas the optimized ReO_3Cl complex on the triplet PES has all three Re=O and Re-Cl bond lengths at 1.701 Å, 1.701 Å, 1.886 Å, and 2.312 Å respectively. On the other hand, the DFT/M06 singlet ReO_3Cl optimized geometry has all Re=O and Re-Cl bonds at 1.693 Å and 2.251 Å respectively whereas its counterpart on the triplet surface has all three Re=O and Re-Cl bonds lengths at 1.690 Å, 1.690 Å, 1.691 Å, and 2.291 Å respectively. The triplet oxo complex showed less stability compared to the singlet structure by 60.90 kcal/mol and 63.89 kcal/mol at DFT/B3LYP and DFT/M06 respectively. As shown in Fig. 1d and e, calculations of the frontier molecular orbitals of the reacting species show that electrons flow from the Highest Occupied Molecular Orbital (HOMO) of the TME into the Lowest Unoccupied Molecular Orbital (LUMO) of the rhenium-oxo complex at both levels of theories.

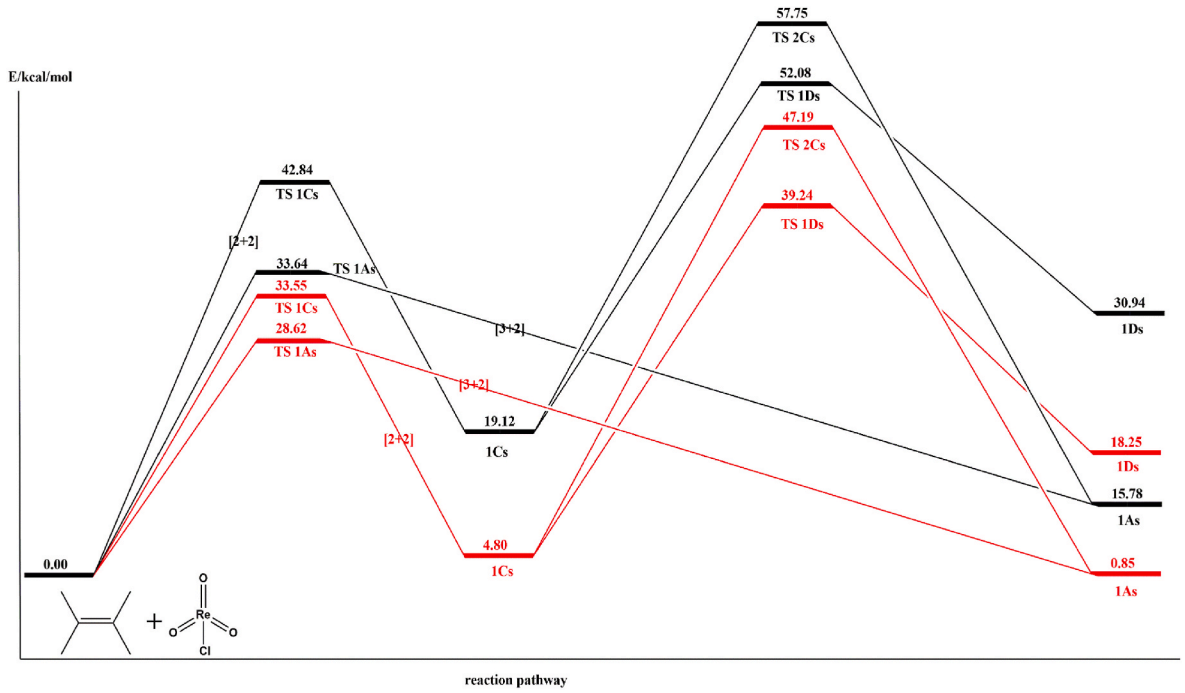

Fig. 1a. Relative Gibbs free energy profile diagram for the reaction between ReO_3Cl and TME on the singlet surface at the DFT/M06/LACVP*(red colour) and DFT/B3LYP/LACVP* (black colour) level of theory. (For interpretation of the references to colour in this figure legend, the reader is referred to the Web version of this article.)

On the singlet concerted PES, the direct [3 + 2] insertion of the olefinic bond across the O=Re=O functionality of the ReO_3Cl complex leads to the formation of [**1As**] intermediate. The DFT/B3LYP free activation and reaction energies associated with this process were 33.64 kcal/mol and 15.78 kcal/mol respectively. Furthermore, the DFT/M06 activation and reaction energies associated with the initial [3 + 2] step were found to be 28.62 kcal/mol and 0.85 kcal/mol respectively. Results from both levels of theory suggest that the formation of the dioxylate intermediate [**1As**] is not a spontaneous process due to the endergonic nature of the oxidation process on the singlet PES. The DFT/B3LYP computed triplet dioxylate intermediate [**1At**] lies 3.62 kcal/mol lower than its singlet counterpart [**1As**] whereas the DFT/M06 singlet dioxylate intermediate [**1As**] was 4.84 kcal/mol more stable than its triplet counterpart [**1At**]. An exhaustive attempt to locate the transition state linking the reactant to the product on the triplet surface proved futile for the [3 + 2] route at both levels of theories.

The stepwise [2 + 2] route *via* the transition state **TS1C** and a **1C** metallaoxetane intermediate **in** Scheme 1, which according to Sharpless et al. [30] re-arranges to the [3 + 2] product was also explored at both levels.

A DFT/B3LYP computed energy barrier of 42.84 kcal/mol needs to be overcome to form the metallaoxetane intermediate **[1Cs]** on the singlet surface. At the DFT/M06 level, the activation barrier for the initial [2 + 2] route on the singlet was 33.55 kcal/mol. There was no transition state located for the [2 + 2] mechanism on the triplet PES at both levels of theory. The computed activation energies at both levels suggest that the free energy of activation for the singlet transition state is high for the [2 + 2] route than for the [3 + 2] route. This observation makes the initial [2 + 2] route unstable over the [3 + 2] route. Furthermore, on the singlet PES, the formation of the singlet metallaoxetane intermediate shows an endergonicity of 19.12 kcal/mol and 4.80 kcal/mol at the B3LYP and M06 levels respectively. The B3LYP triplet metallaoxetane intermediate **[1Ct]** was located and found to be 16.83 kcal/mol less stable than the singlet counterpart **[1Cs]** whereas the M06 singlet metallaoxetane intermediate **[1Cs]** was located and found to be 22.27 kcal/mol less stable than the triplet counterpart. The optimized B3LYP transition state **[TS 1Cs in** Scheme 1**]** from the [2 + 2] pathway has its newly forming C–O and Re-C bonds at 1.963 Å and 2.256 Å respectively. On the singlet PES, the computed M06 saddle point structure from the [2 + 2] pathway has its newly forming C–O and Re-C bonds at 2.070 Å and 2.367 Å respectively.

The free activation energy computed for the formation of the dioxylate intermediate **[1As]** on the singlet surface through the saddle point structure **[TS-2Cs in** Scheme 1**]** was 57.75 kcal/mol and 47.19 kcal/mol at the B3LYP and M06 respectively. There was no transient structure **[TS-2Ct in** Scheme 1**]** optimized from the triplet surface at the B3LYP level. This observation was confirmed by the M06 computations. Due to the kinetic hindrance of the [2 + 2] route, that is, the high activation barrier of the initial [2 + 2] step, and the endergonic nature of the formation of the [2 + 2] intermediate, the formation of diols favours the [3 + 2] pathway in terms of energetics as shown in Fig. 1a.

The possibility of epoxidation *via* the transition state **[TS-1Ds in** Scheme 1**]** was explored at both levels of theory and was computed to have free activation and reaction energies of 52.08 kcal/mol and 30.94 kcal/mol at the B3LYP level and 39.24 kcal/mol and 18.25 kcal/mol at the M06 level respectively on the singlet PES. The B3LYP singlet epoxide **[1Ds]** was computed to lie lower than its triplet counterpart **[1Dt]** by 10.07 kcal/mol. On the other hand, the M06 singlet epoxide **[1Ds]** was computed to lie lower than its triplet counterpart **[1Dt]** by 11.50 kcal/mol. Similar to the observation on the [3 + 2] and [2 + 2] triplet PES at both levels of theory, no transition state **[TS 1Dt in** Scheme 1**]** was found. After an exhaustive search on the PES, it was observed that epoxidation *via* transients **[TS-1B and TS-2A in** Scheme 1**]** was not possible on the singlet and triplet surfaces at both levels of theory. This indicates that the formation of an epoxide by the oxidation of TME mediated by the ReO_3Cl catalyst occurs only *via* the [2 + 2] route. The [2 + 1] route or the re-arrangement of the dioxylate intermediate is not possible as evident from the computations.

Efforts to optimize saddle point structures from the stepwise reaction mechanism proved futile for all pathways on both singlet and triplet surfaces at both levels of theory. This indicates that the oxidation of TME catalyzed by the rhenium oxide will proceed *via* the concerted [3 + 2]

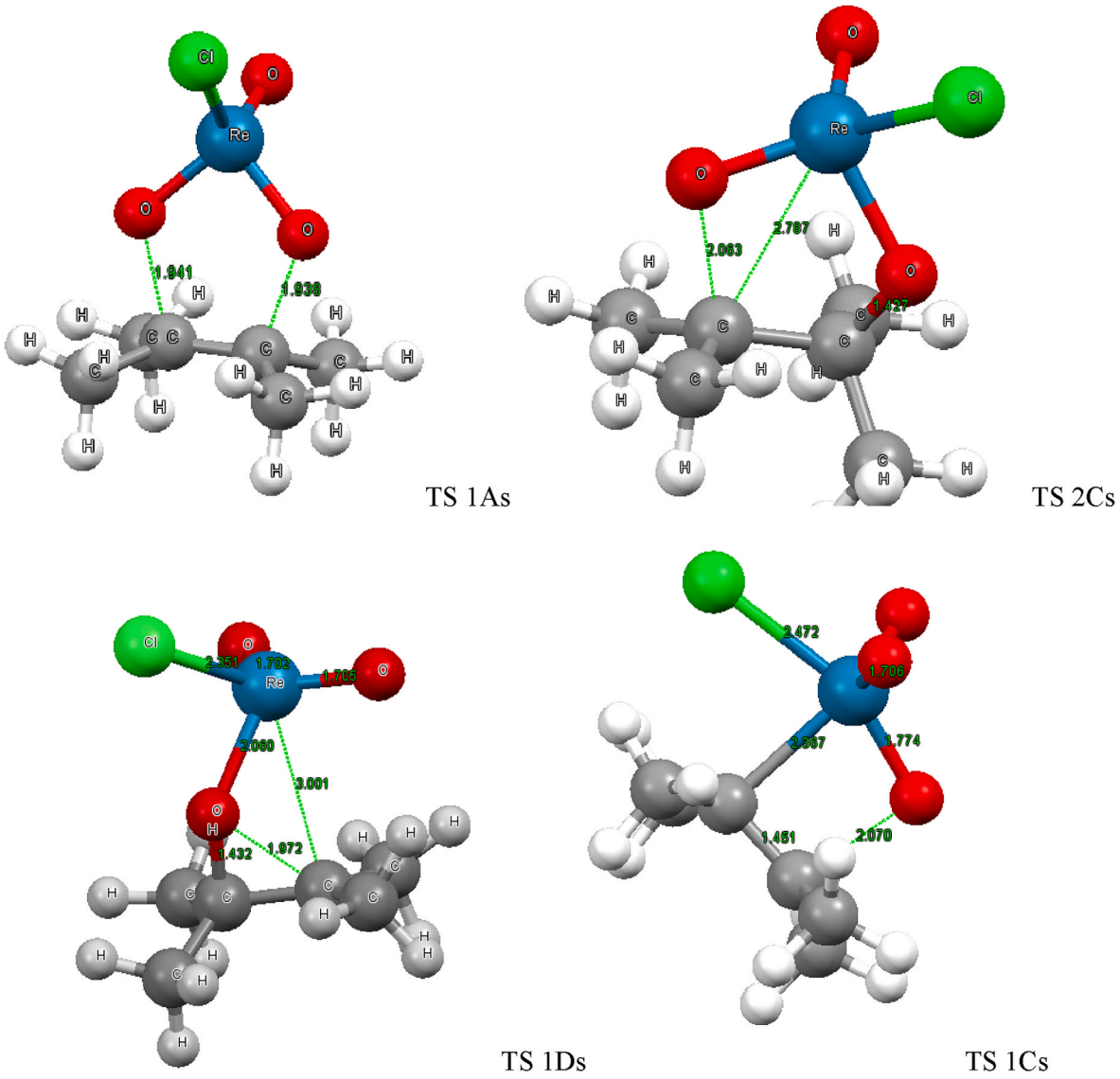

Fig. 1b. Optimized transition states involved in the reaction between ReO_3Cl and TME on the singlet surface at the DFT/M06/LACVP* level of theory. The colour code for atoms; Red = Oxygen, Green = Chlorine, Grey = Carbon, White = Hydrogen, and Blue = Rhenium. (For interpretation of the references to colour in this figure legend, the reader is referred to the Web version of this article.)

route in terms of dioxylation and the concerted [2 + 2] route in terms of epoxidation. It can therefore be said that the formation of diols and epoxides from the oxidation of TME mediated by the rhenium oxide complex is not a spontaneous process at 298.15 K and 1 atm.

2.2. Reaction of TcO_3Cl with TME

The relative energy profiles, saddle point structures optimized from the singlet PES and HOMO-LUMO energy gaps are shown in Fig. 2a–e respectively.

The M06 and B3LYP optimized technetium oxide complex on the single PES was found to be chiral since ground state optimization at both levels of theories yielded a C_1 point group. The B3LYP geometry optimization of the TcO_3Cl molecular system yielded Tc=O and Tc-Cl bond distances of 1.698 Å and 2.262 Å respectively. On the other hand, the triplet optimized TcO_3Cl complex had geometry with all three Tc=O and Tc-Cl bond distances at 1.693 Å, 1.726 Å, 1.873 Å, and 2.280 Å respectively. Furthermore, the M06 optimized TcO_3Cl complex had its Tc=O and Tc-Cl bond distances at 1.687 Å and 2.249 Å respectively, and Tc=O and Tc-Cl bond distances at 1.699 Å, 1.683 Å, 1.895 Å, and 2.269 Å respectively for the optimized triplet geometry. At both levels of theory, the singlet structure was stable over its triplet counterpart (>46.00 kcal/mol). As evident from Fig. 2d and e, the movement of electrons from the (HOMO) of the TME into the (LUMO) of the TcO_3Cl is favoured at all levels of theory compared to vice versa. Hence, in the oxidation of TME assisted by TcO_3Cl, electrons will flow from the TME into the d orbitals of the technetium complex.

From the stepwise reaction mechanism **(blue coloured in** Scheme 1**)**, the formation of the organometallic intermediate **(1Xs intermediate in** Scheme 1**)** is an endergonic process per the B3LYP results and exergonic per M06 calculations with Gibbs free energies at 13.64 kcal/mol and −2.14 kcal/mol respectively. The computed B3LYP and M06 activation energies for the formation of the **intermediate 1Xs in** Scheme 1 were found to be 25.58 kcal/mol and 17.59 kcal/mol respectively on the singlet surface. As illustrated in Fig. 2a, the formation of the singlet dioxylate intermediate, **1As [**Scheme 1] *via* the rearrangement of the intermediate, **1Xs** through the transient **TS-[2Xs]** has to overcome free activation energy of 33.23 kcal/mol and 23.19 kcal/mol at the B3LYP and M06 level respectively. No transition state [TS3X and TS-4X] could be located on both singlet and triplet surfaces for the formation of an

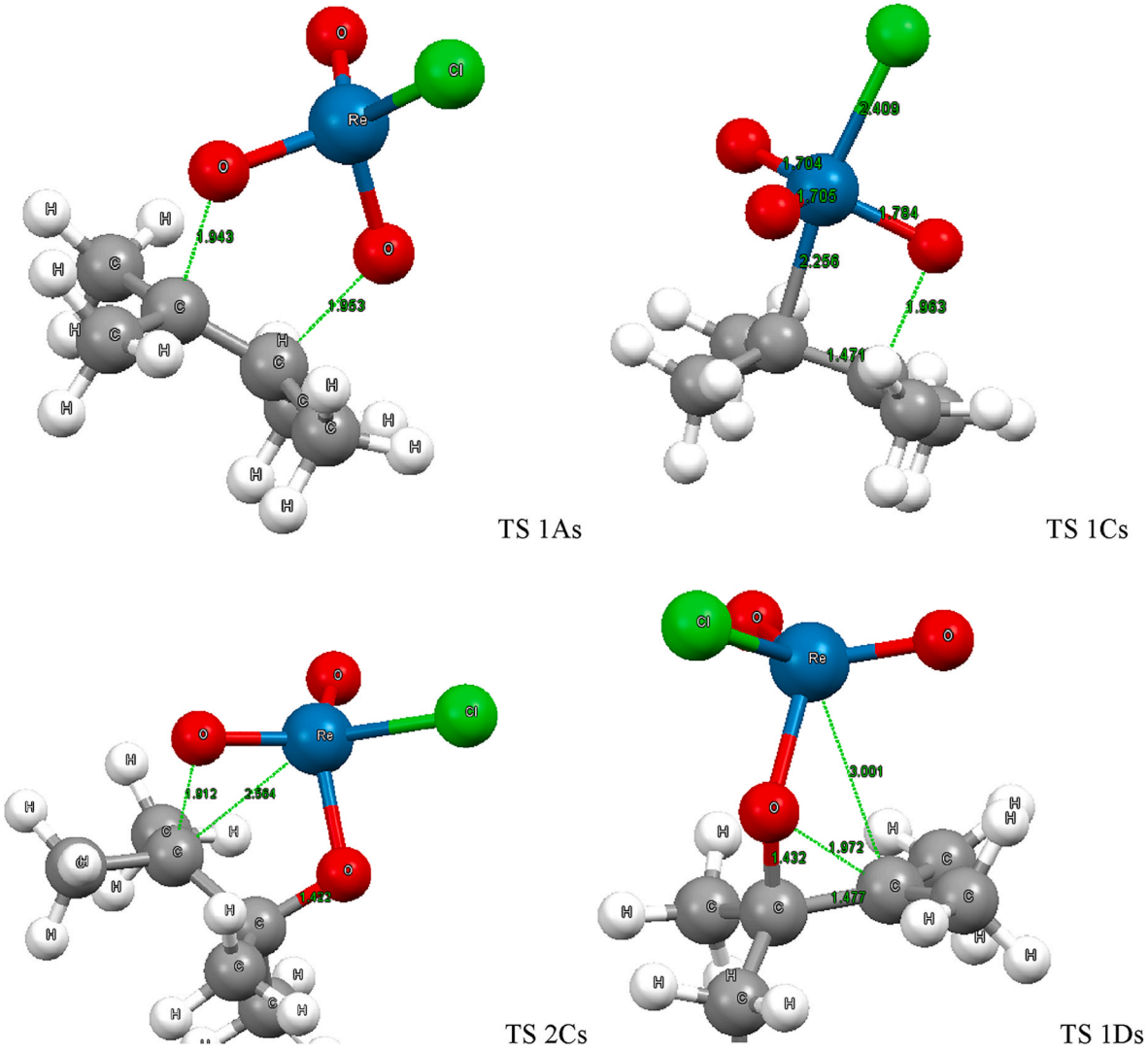

Fig. 1c. Optimized transition states involved in the reaction between ReO_3Cl and TME on the singlet surface at the DFT/B3LYP/LACVP* level of theory. The colour code for atoms; Red = Oxygen, Green = Chlorine, Grey = Carbon, White = Hydrogen, and Blue = Rhenium. (For interpretation of the references to colour in this figure legend, the reader is referred to the Web version of this article.)

epoxide and the metallaoxetane intermediate respectively at both levels of theory.

Dioxylation resulting from the concerted reaction mechanism on the singlet surface **([3 + 2] route in** Scheme 1**)** needs to overcome an activation barrier of 18.25 kcal/mol and 13.02 kcal/mol at the B3LYP and M06 levels of theories respectively. The Gibbs free energies computed at the M06 and B3LYP levels for the [3 + 2] **(route in** Scheme 1**)** are −27.03 kcal/mol and −13.14 kcal/mol respectively on the singlet PES.

As compared to the dioxylation abilities of ReO_3Cl **(discussed in** section 3.1**)**, the dioxylation process catalyzed by TcO_3Cl is spontaneous at 298.15 K as evident from the calculations and illustrated in Fig. 2a. It was found that the B3LYP computed triplet dioxylate intermediate **[1At]** lies 1.53 kcal/mol lower than its singlet structure **[1As]**. This story did not differ from that of the M06 level where the singlet dioxylate intermediate **[1As]** was also 1.75 kcal/mol more stable than its triplet counterpart **[1At]**. Efforts to explore the reaction surface to optimize the triplet saddle point structure for the [3 + 2] route proved futile at both levels of theory.

A competing reaction process; that is the formation of metallaoxetane intermediate *via* the transition state **TS1C in** Scheme 1, was explored on both singlet and triplet surfaces at the B3LYP and M06 levels of theory. From the B3LYP computations on the singlet surface, the metallaoxetane formation was 20.70 kcal/mol endergonic and was computed to have an activation barrier of 47.73 kcal/mol. The energetics computed at the M06 agrees with that at the B3LYP with activation and Gibbs free energies of 4.46 kcal/mol and 35.38 kcal/mol respectively on the singlet PES. The nature of the energetics computed for the metallaoxetane formation route on the singlet PES rules out its formation on the singlet surface due to the thermodynamic and kinetic instability as compared to the [3 + 2] pathway. On the triplet surface, no transition state is located for the [2 + 2] reaction mechanism at both levels of theory. Geometry optimization of the metallaoxetane intermediate **[1C]** at the B3LYP level of theory showed that the singlet metallaoxetane intermediate was stable over its triplet structure by 33.10 kcal/mol whereas the M06 triplet metallaoxetane intermediate lay 23.46 kcal/mol below its counterpart on the singlet PES.

The computations at the B3LYP and M06 levels of theory showed that dioxylation *via* the [2 + 2] route through the rearrangement of the metallaoxetane intermediate *via* the saddle point geometry **[TS-2Cs in** Scheme 1**]** needed to overcome an activation barrier of 37.22 kcal/mol and 23.09 kcal/mol respectively. Efforts to optimize a transient **[TS-2Ct in** Scheme 1**]** from the triplet PES at both levels of theory proved futile. Based on the energetics computed at both levels for all routes leading to

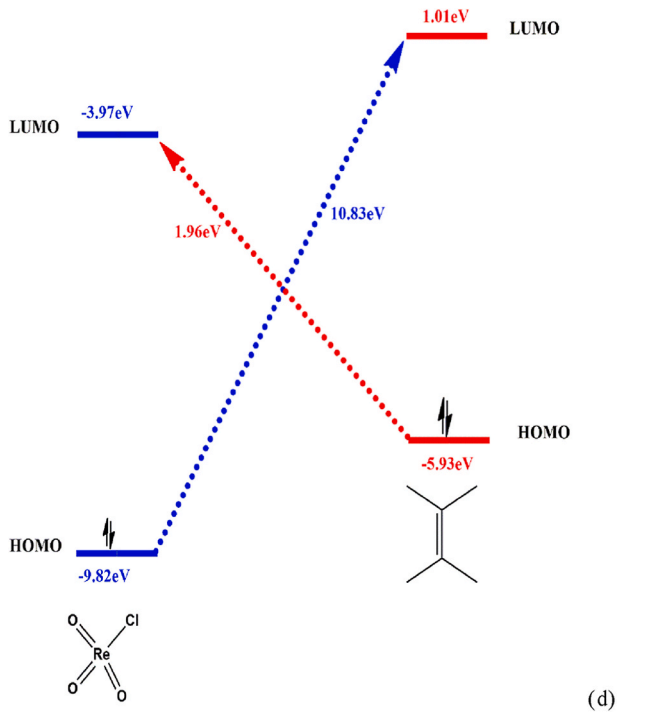

Fig. 1d. Graphical representation of the interaction between the frontier molecular orbitals between the ReO_3Cl complex and TME on the singlet surface at the DFT/B3LYP/LACVP* level of theory.

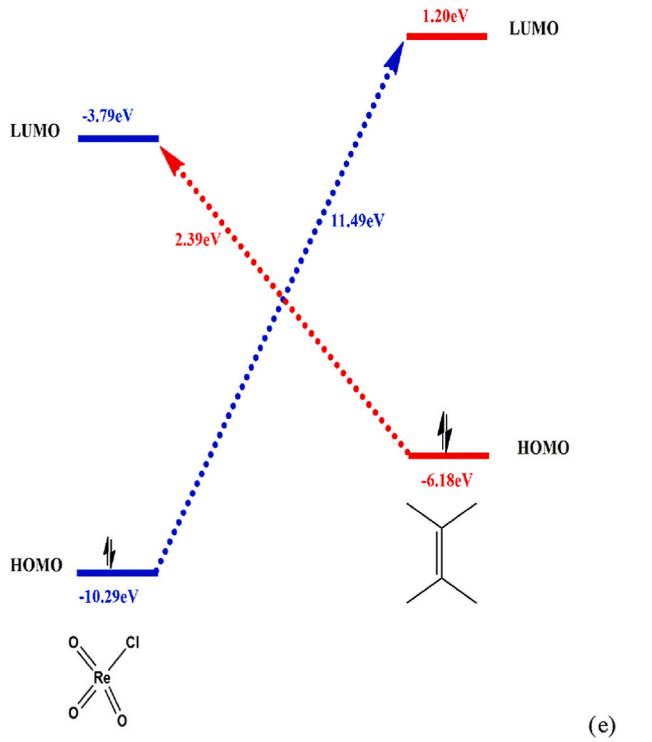

Fig. 1e. Graphical representation of the interaction between the frontier molecular orbitals between the ReO_3Cl complex and TME on the singlet surface at the DFT/M06/LACVP* level of theory.

dioxylation, the [2 + 2] route is not favoured for dioxylation due to the kinetic and thermodynamic factors.

Epoxidation *via* the transient **[TS-1Ds in** Scheme 1**]** was explored at both levels of theory on the singlet and triplet PES. On the singlet surface at the B3LYP level, the computed free activation and reaction energies of the barrier were 29.16 kcal/mol and 4.82 kcal/mol whereas an activation barrier and Gibbs free energy of 16.66 kcal/mol and −6.12 kcal/mol respectively were computed at the M06 level. Again as observed in section 3.1, the B3LYP optimized singlet epoxide **[1Ds]** was computed to be more stable than its triplet structure **[1Dt]** at all levels of theory (>6.0 kcal/mol). Furthermore, on the singlet and triplet surfaces, it was observed at both levels of the theory that epoxidation *via* the saddle point geometries **[TS-1B and TS-2A in** Scheme 1**]** were not possible. Hence, it can be inferred that epoxidation of TME will proceed *via* the [2 + 2] reaction mechanism on the singlet surface. Results from the oxidation of TME catalyzed by TcO_3Cl at both levels of the theory suggest that hydroxylation **[3 + 2]** and epoxidation **[2 + 2]** will likely proceed *via* the concerted route and not stepwise.

2.3. Reaction of MnO_3Cl with TME

Illustrated in Fig. 3a–e respectively are the relative free energy profiles, optimized transients optimized from the singlet PES and the HOMO-LUMO energies between the reactants.

Optimization of the singlet permanganyl chloride complex at both levels of theory yielded a tetrahedron geometry with C_1 symmetry. Similar to the observations in sections 3.1 and 3.2, the permanganyl chloride was found to be chiral due to the absence of all symmetry elements except the identity operation (E). As shown in Fig. 3d (B3LYP calculations) and 3e (M06 calculations), the movement of electrons from the TME molecular system into the d orbitals of the manganese metal of the permanganyl chloride complex on the singlet PES is favoured energetically over vice versa.

The B3LYP optimized permanganyl chloride geometry has all Mn=O and Mn–Cl bond lengths equal to 1.558 Å and 2.127 Å respectively whereas the triplet MnO_3Cl complex on the triplet PES has all the three Mn=O and Mn–Cl bond lengths at 1.723 Å, 1.552 Å, 1.556 Å, and 2.124 Å respectively. Furthermore, the MnO_3Cl complex has all Mn=O and Mn–Cl bond lengths equal to 1.550 Å and 2.106 Å respectively whereas the triplet MnO_3Cl complex on the triplet PES has all the three Mn=O and Mn–Cl bond lengths at 1.744 Å, 1.550 Å, 1.549 Å, and 2.103 Å respectively at the M06 level of theory. As observed in sections 3.1 and 3.2, the triplet oxo complex showed less stability compared to the singlet structure (<20.00 kcal/mol) at both levels of theory.

The formation of epoxides on the singlet PES from the manganoxetane and dioxomangana-2,5-dioxolane intermediate precursors was explored at both levels of theory on the singlet and triplet surfaces. However, no transient structure **[TS-2A and TS-1D in** Scheme 1**]** could be optimized from both the singlet and triplet PES at both levels. Moreover, it was observed that epoxidation *via* the transition state **[TS-1Bs in** Scheme 1**]** is an exergonic process (−27.38 kcal/mol, B3LYP) (−30.40 kcal/mol, M06). The free activation barrier was computed to be 6.06 kcal/mol and 0.67 kcal/mol at the B3LYP level and M06 level respectively on the singlet PES. On the singlet surface, it was observed that the B3LYP epoxide **[1Ds]** was found to lie lower than its triplet structure **[1Dt]** by 5.50 kcal/mol. On the other hand, the M06 triplet epoxide **[1Ds]** was also found to lie lower than its singlet counterpart **[1Dt]** by 15.67 kcal/mol. The nature of stability of stationary points as discussed in sections 3.1 and 3.2 was similar to this observation. This tells us that this oxidation of TME mediated by permanganyl chloride will likely occur on the singlet surface. No saddle point structure be optimized for all other concerted reaction mechanisms ([3 + 2] and [2+]) at both levels of theory on the singlet and triplet surface. This tells us that permanganyl chloride will exclusively epoxide TME at 298.15 K and 1atm. A similar observation was made by Fosu et al. [31] who predicted the manganese oxo complex of the type, MnO_3L (L = F-) to exclusively epoxide on the singlet surface at 298.15 K and 1 atm.

Along the stepwise pathway, one of the C=C π bonds of TME attacks an oxo-ligand of the permaganyl chloride complex to form the organometallic intermediate **[1Xs] in** Scheme 1. As shown in the Gibbs free

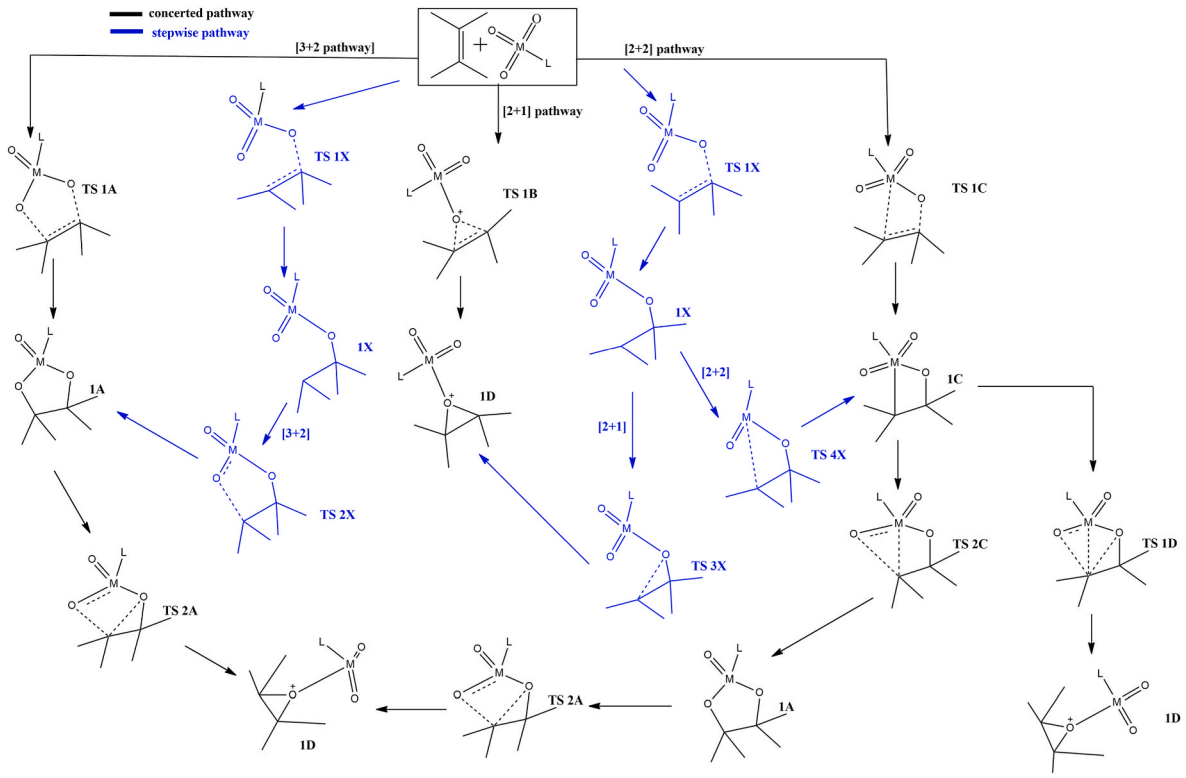

Scheme 1. A proposed mechanistic pathway for the addition of MO_3Cl [M = Mn, Tc, and Re] to tetramethylethylene (TME).

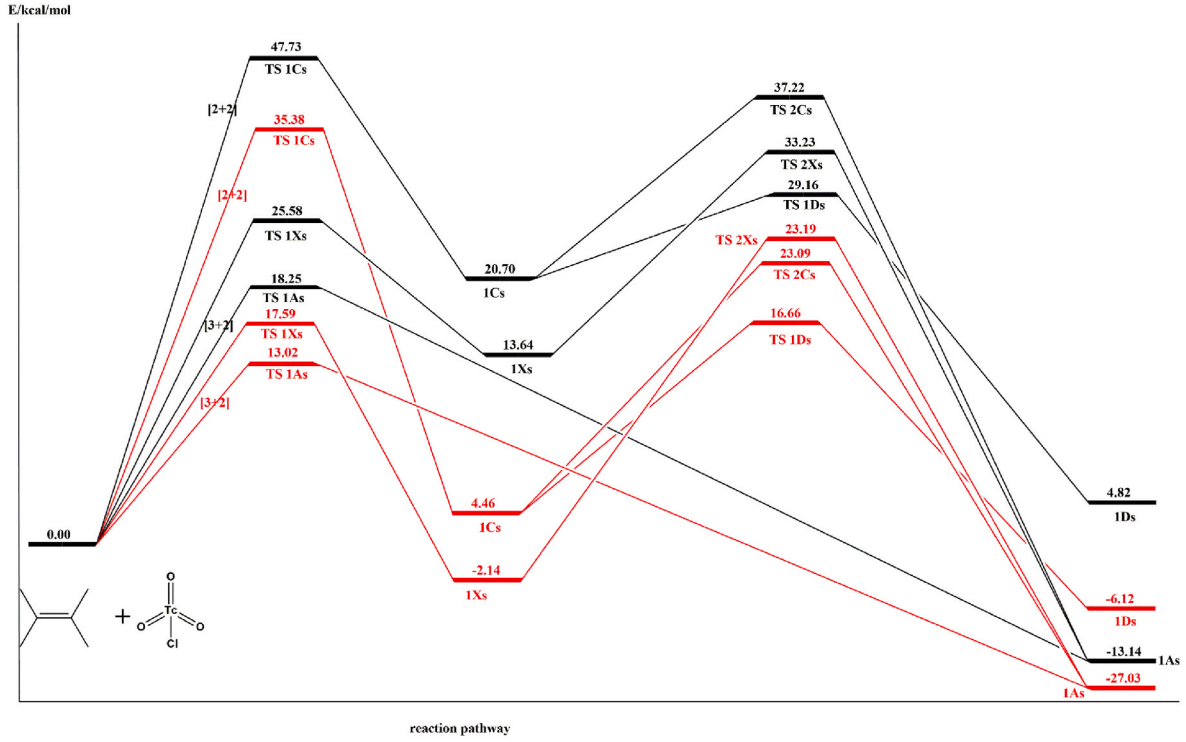

Fig. 2a. Relative Gibbs free energy profile diagram for the reaction between TcO_3Cl and TME on the singlet surface at the DFT/M06/LACVP*(red colour) and DFT/B3LYP/LACVP* (black colour) level of theory. (For interpretation of the references to colour in this figure legend, the reader is referred to the Web version of this article.)

energy profile (Fig. 3a), the formation of the **intermediate 1Xs in** Scheme 1 is highly spontaneous, however, the organometallic intermediate **[1Xs]** could not act as a precursor for the formation of epoxide, manganoxetane, and dioxomangana-2,5-dioxolane at both levels of theory on the singlet and triplet PES. The nature of the energetics on the PES of the oxidation of TME by permanganyl chloride points out that the

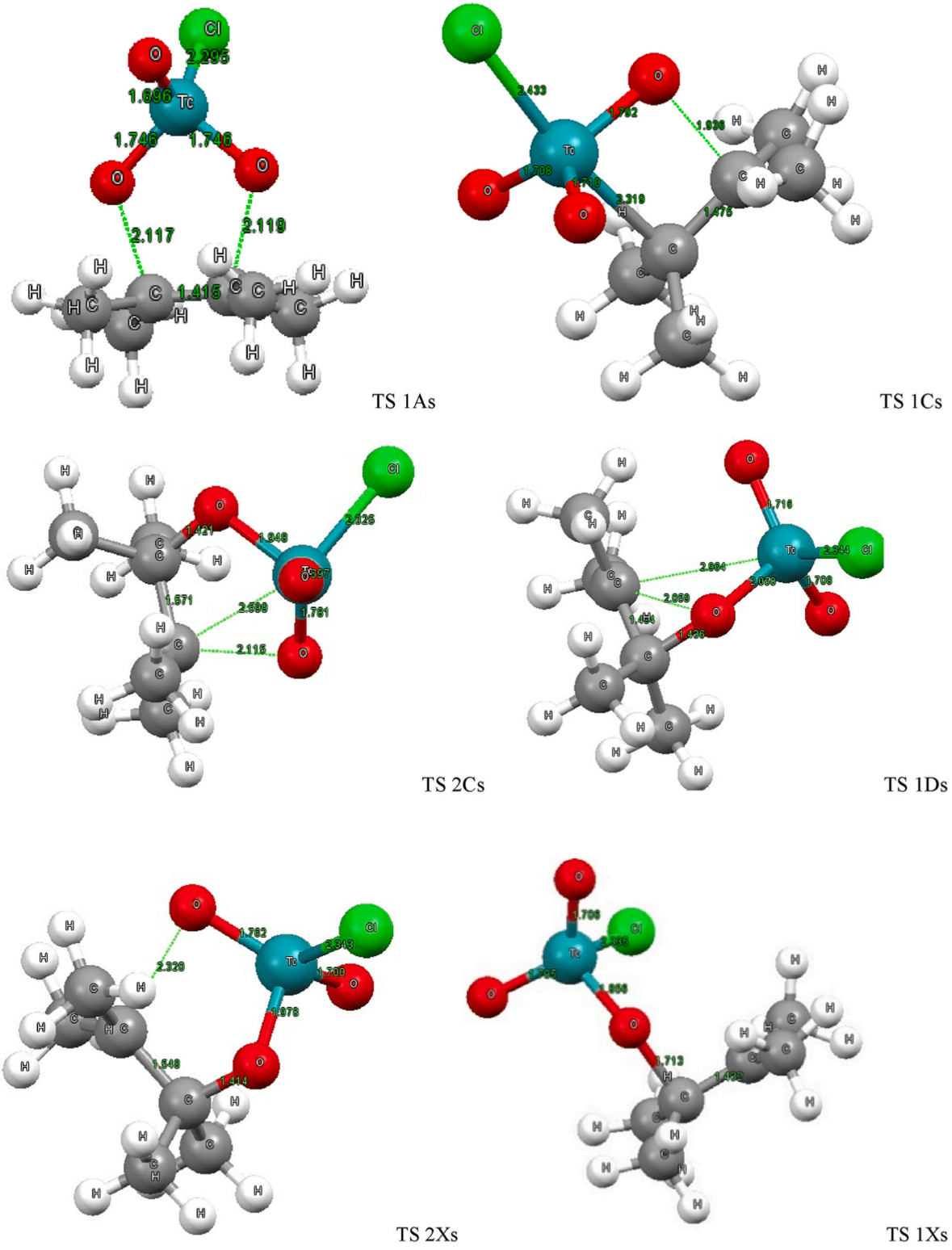

Fig. 2b. Optimized transition states involved in the reaction between TcO_3Cl and TME on the singlet surface at the DFT/M06/LACVP* level of theory. The colour code for atoms; Red = Oxygen, Green = Chlorine, Grey = Carbon, White = Hydrogen, and Green = Technetium. (For interpretation of the references to colour in this figure legend, the reader is referred to the Web version of this article.)

manganese oxide complex will predominantly lead to epoxidation at 298.15 K confirming the experimental study by Wistuba et al. [24].

2.4. Global and local reactivity indices calculations on the singlet PES

In this quantum chemical study, the global electrophilicity index (ω) and maximum electronic charge (ΔN_{max}) of the metal oxo complexes and the TME molecular system on the singlet PES were calculated using equations (1) and (2) respectively.

$$\omega = \mu^2/2\eta \quad (1)$$

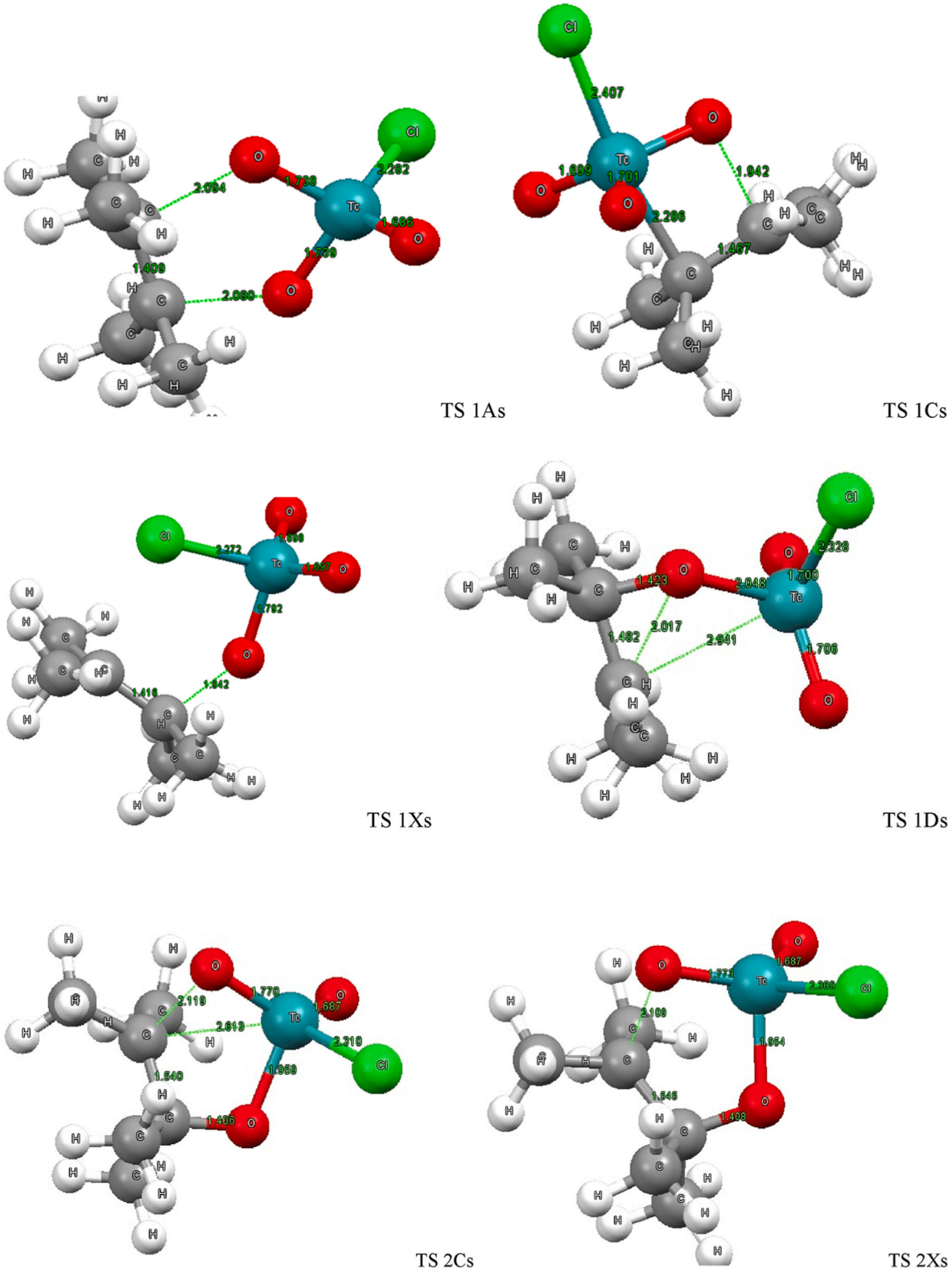

Fig. 2c. Optimized transition states involved in the reaction between TcO_3Cl and TME on the singlet surface at the DFT/B3LYP/LACVP* level of theory. The colour code for atoms; Red = Oxygen, Green = Chlorine, Grey = Carbon, White = Hydrogen, and Green = Technetium. (For interpretation of the references to colour in this figure legend, the reader is referred to the Web version of this article.)

$$\mathbf{\Delta Nmax} = -\mu/\eta \tag{2}$$

The electrophilicity indexes quantitatively predict the electron-accepting nature of reacting species on reaction surfaces [32]. As shown in equation (1), it is dependent on electronic properties such as the electronic chemical potential μ [Eq. (3)], and chemical hardness [33], η [Eq. (4)]

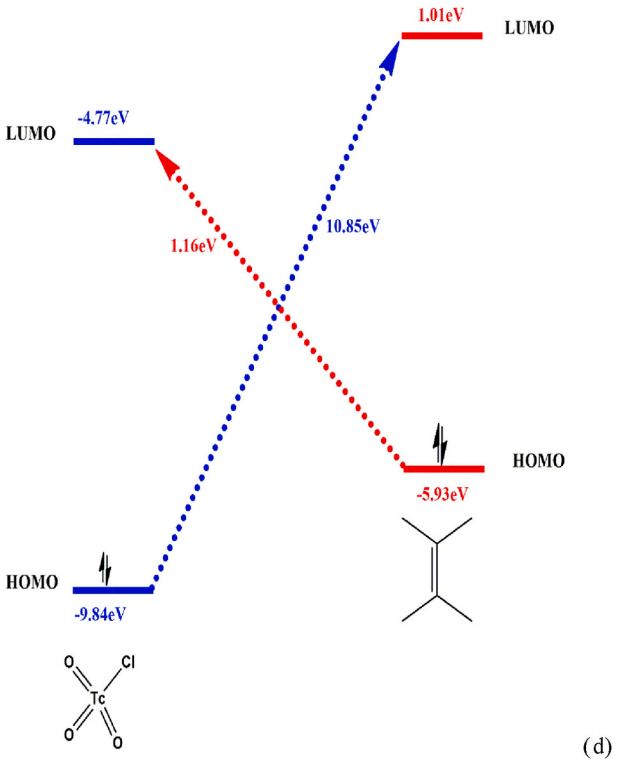

Fig. 2d. Graphical representation of the interaction between the frontier molecular orbitals between the TcO_3Cl complex and TME on the singlet surface at the DFT/B3LYP/LACVP* level of theory.

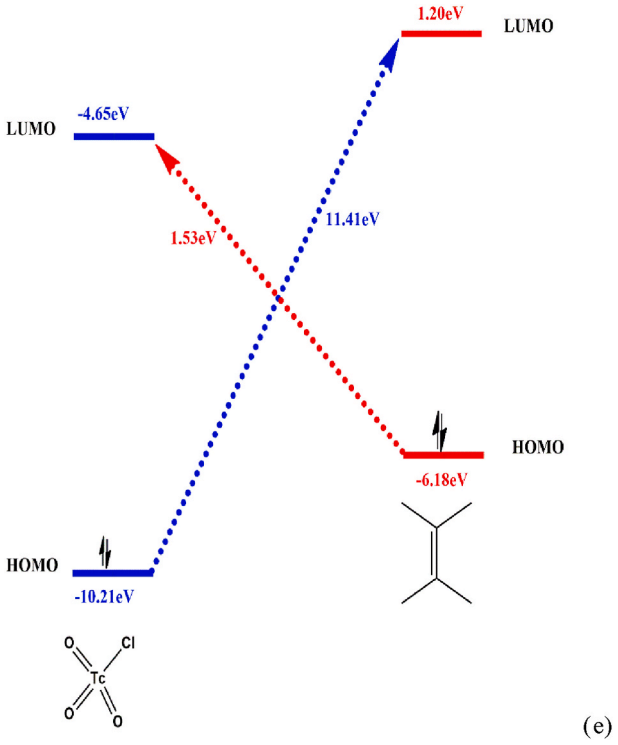

Fig. 2e. Graphical representation of the interaction between the frontier molecular orbitals between the TcO_3Cl complex and TME on the singlet surface at the DFT/M06/LACVP* level of theory.

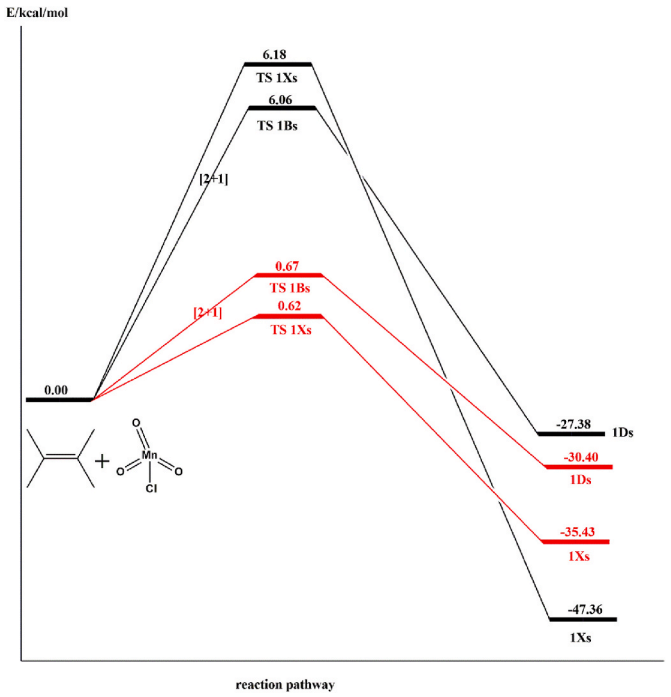

Fig. 3a. Relative Gibbs free energy profile diagram for the reaction between MnO_3Cl and TME on the singlet surface at the DFT/MO6/LACVP*(red colour) and DFT/B3LYP/LACVP* (black colour) level of theory. (For interpretation of the references to colour in this figure legend, the reader is referred to the Web version of this article.)

$$\mu = \frac{HOMO + LUMO}{2} \tag{3}$$

$$\eta = [LUMO] - [HOMO] \tag{4}$$

Hence, molecular structures that have large electrophilicity values will tend to be more reactive toward nucleophilic centres on the reaction surface in a given set of reagents. These equations are based on the Koopmans theory [34] originally established for calculating ionization energies from closed-shell Hartree–Fock wavefunction but have since been adopted as acceptable approximations for computing electronic chemical potential and chemical hardness. Furthermore, the maximum electronic charge transfer (ΔN_{max}) estimates the maximum electronic charge that an electrophile may accept. This means that molecular systems with large ΔN_{max} index would be the best electrophile for a given series of compounds. The ΔN_{max} values for all transition metal oxo complexes are greater than that of the TME system on the singlet PES. This indicates that on the reaction surfaces the transition metal oxo complexes will be electrophiles as shown in Table 1 at both levels of theories.

As evident from Table 1, all the transition metal oxo complexes have a lower chemical potential (μ) compared to the TME molecular system on the singlet PES at both levels of theories. This suggests that electrons will tend to easily move from the olefinic systems to the metal complexes on the singlet PES. At both levels of theories, it is evident that the TME geometry has the largest chemical potential value indicating that it will be easy to liberate electrons from the TME system to the metal oxo complexes on the singlet PES. This indicates that TME is the nucleophile and the metal oxo complexes are the electrophiles. These results support the observation made with the frontier molecular orbital calculations.

Furthermore, the permanganyl chloride has the highest electrophilicity index value followed by the technetium and rhenium oxide complexes. This electronic nature indicates that the permanganyl complex will be the likely complex to easily accept electrons from the olefins with the rhenium oxide complex being the least.

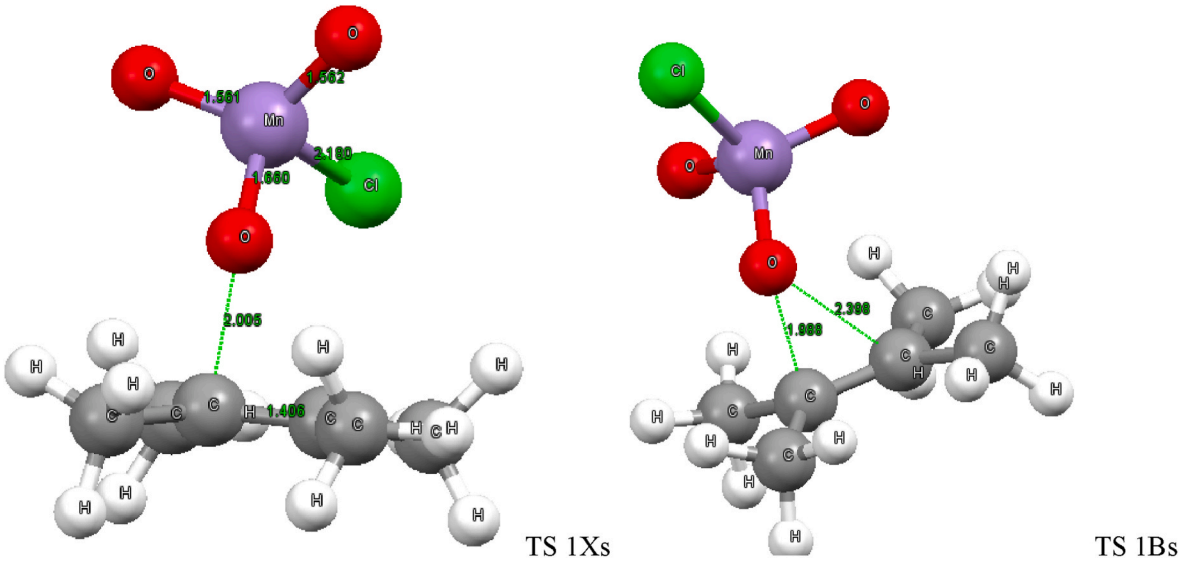

Fig. 3b. Optimized transition states involved in the reaction between MnO_3Cl and TME on the singlet surface at the DFT/M06/LACVP* level of theory. The colour code for atoms; Red = Oxygen, Green = Chlorine, Grey = Carbon, White = Hydrogen, and Voilet = Manganese. (For interpretation of the references to colour in this figure legend, the reader is referred to the Web version of this article.)

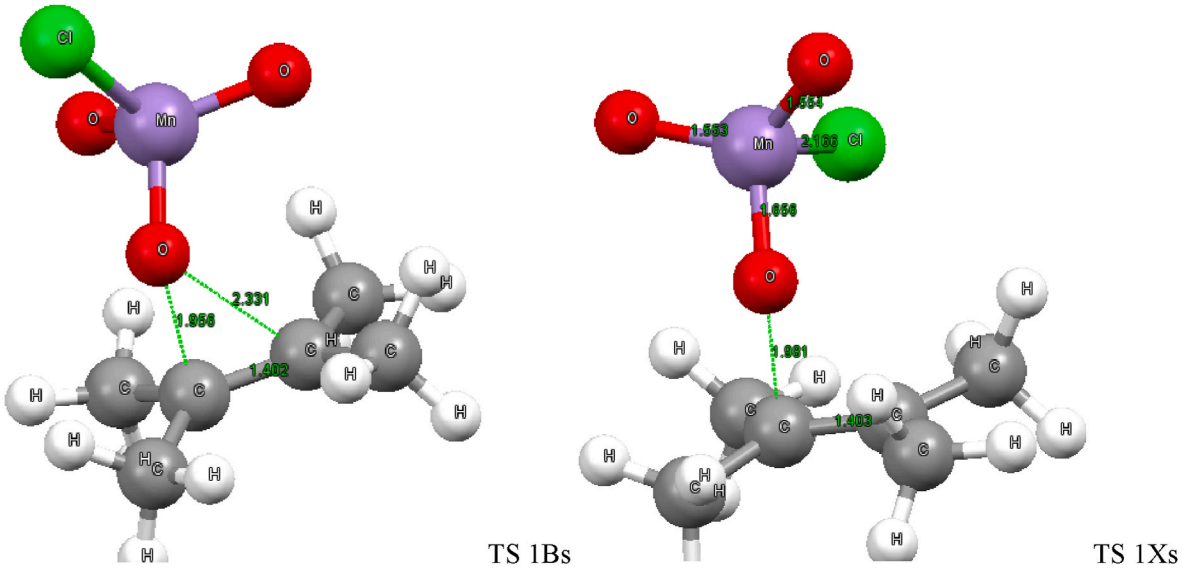

Fig. 3c. Optimized transition states involved in the reaction between MnO_3Cl and TME on the singlet surface at the DFT/B3LYP/LACVP* level of theory. The colour code for atoms; Red = Oxygen, Green = Chlorine, Grey = Carbon, White = Hydrogen, and Voilet = Manganese. (For interpretation of the references to colour in this figure legend, the reader is referred to the Web version of this article.)

This observation can also be related to the activation and reaction energies on the reaction surface with the most electrophilic system being the most reactive and thus having the lowest activation and reaction energies. This further explains why the rhenium oxide addition route has the highest activation and reaction energies and the permanganyl chloride catalyzed route has the lowest activation and reaction energies on the singlet PES.

2.5. Temperature changes effects on the oxidation strengths of MO_3Cl (M = Mn, Tc, and Re)

The reaction temperature was varied to 323.15 K (50 °C) and 373.15 K (100 °C) after the reaction was studied at room temperature (298.15 K, 25 °C). The reaction and activation energies along the reaction pathway for each catalyzed route structure can be found in Tables S4–S9. This was done to study the effects of temperature changes on the reaction properties (kinetics and thermodynamics) of the addition of MO_3Cl (M = Mn, Tc, and Re) to tetramethylethylene on both singlet and triplet PES at both levels of theories (M06 and B3LYP).

At both levels of theory (M06 and B3LYP), it was observed that in cases where no stationary points could be optimized from both singlet and triplet PES at 298.15 K, the observation was the same when the temperatures were elevated to 323.15 K and 373.15 K. For example, as seen in Table S4, there are no activation energy barriers observed for the concerted [2 + 1] and the stepwise mechanistic route [TS-1X] at all temperatures.

Generally, it was observed that the free activation and reaction energies increased when the temperature was changed from 298.15 K to 373.15 K on the singlet PES as shown in Tables S4–S9. This observation, therefore, tends to suggest that at elevated temperatures the oxidation

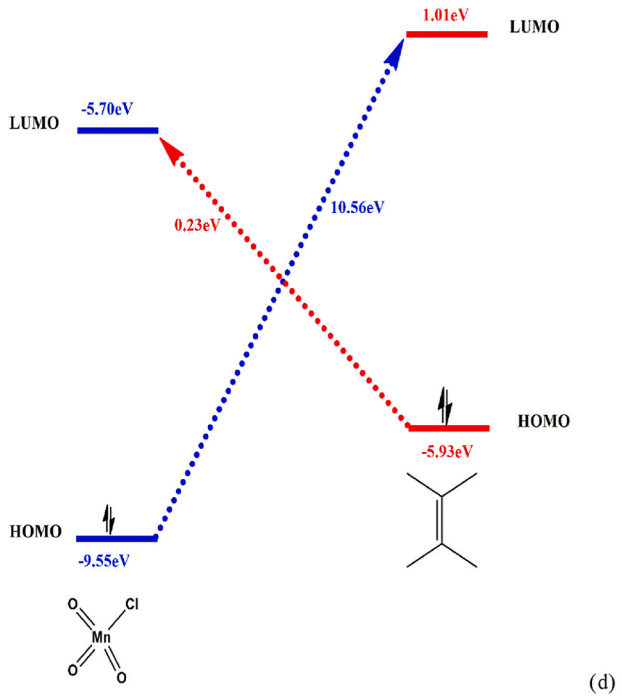

Fig. 3d. Graphical representation of the interaction between the frontier molecular orbitals between the MnO_3Cl complex and TME on the singlet surface at the DFT/B3LYP/LACVP* level of theory.

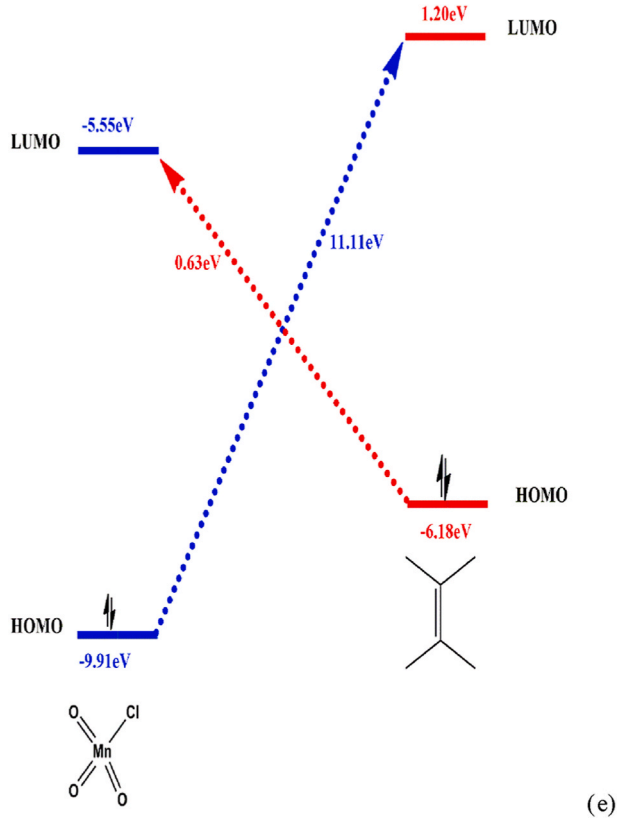

Fig. 3e. Graphical representation of the interaction between the frontier molecular orbitals between the MnO_3Cl complex and TME on the singlet surface at DFT/M06/LACVP* level of theory.

reaction becomes more kinetically and thermodynamically unstable. This could be attributed to the fact that at elevated temperatures, the catalyst deactivates or decomposes hence affecting the fate of the reaction. As evident from Tables S4–S9, the oxidation reaction will be suitable to perform at 298.15 K and 1 atm for maximum yield of products. Moreover, the stabilities of the reaction pathways did not change as all mechanistic channels were still not favoured thermodynamically and kinetically at varying temperatures for all catalyzed surfaces. Furthermore, from the computations at both levels of theories, the reaction mechanism favoured the concerted reaction mechanism over the stepwise reaction pathways at elevated temperatures.

As shown in Tables S4–S9, the preferred reaction mechanism in terms of dioxylation was *via* the [3 + 2] mechanistic channel respectively where plausible. Similar to what was observed in sections 3.1-3.3, all singlet stationary points were computed to be stable over their triplet counterparts at the elevated temperatures except with the formation of dioxomangana-2,5-dioxolane intermediate where the vice versa occurs at both levels of theories.

It was observed that the temperature changes did not affect the nature of the bonding of the reacting species between 298.15 K and 373.15 K as electrons still flowed from the HOMO of the tetramethylethylene (TME) molecule into the LUMO of the metal oxo complexes in all cases.

2.6. Rate constants (k) calculations of the main mechanistic pathways

The rate constants of all considered reaction pathways at 298.15 K were calculated for all catalyzed singlet reaction surfaces at both levels of theories using equation (5) [35,35,36].

$$k[T] = \frac{K\beta T}{h^{\circ}C} e^{\frac{-\Delta G^{\circ}}{RT}} \quad (5)$$

where $K_B = 1.380662 \times 10^{-23}$ J/K is Boltzmann's constant, T = 298.15 K is the reaction temperature, h = 6.62617×10^{-34} Js is Planck's constant, R = 1.987 cal/mol.K is the molar gas constant, ΔG° is the Gibbs free energy of activation, and °C is the concentration of the reacting species which is taken as 1 M.

In Tables 2–4, the [3 + 2] rate constant values represent k values for the initial [3 + 2] route, the $[2 + 2]_a$ values represent the rate constants for the initial [2 + 2] route and the [2 + 1] values give the rate constant for the direct addition leading to epoxidation. Furthermore, the $[2 + 2]_b$ and $[2 + 2]_c$ values show the rate constant values for the mechanistic channels for the conversion of the metallaoxetane intermediate into dioxylate intermediate and epoxides respectively on the singlet PES. The rate constant values for the formation of the organometallic intermediate [1Xs] are also shown in Tables 2–4 From Tables 2 and 3, it is clear that the fastest reaction mechanism among all pathways studied is the [3 + 2] mechanistic route leading to dioxylation on the singlet PES since the rate constant in both cases is the highest compared to other competing routes. Furthermore, the [2 + 2] route is a relatively slow reaction process due to low reaction rate constant values for both the rhenium and technetium-catalyzed surfaces. The stepwise process leading to the formation of the 1X intermediate from the technetium oxide catalyzed surface as shown in Table 3 is a moderately fast reaction. This makes it a competing process kinetically with the [3 + 2] route.

The rhenium oxide catalyzed surface [3 + 2] route is 5.58×10^6 **(B3LYP)** or 4.11×10^3 **(M06)** faster than the [2 + 2] route whereas the [3 + 2] reaction mechanism is 4.09×10^{21} **(B3LYP)** or 2.46×10^{16} **(M06)** faster than the [2 + 2] route on the technetium oxide catalyzed singlet PES.

For the epoxidation process seen in the case of the oxidation TME by the permanganyl chloride (results in Table 4), the reaction mechanism is very fast due to the high-rate constant value at 298.15 K. In all cases, the rate constants from the M06 simulations were higher than that of B3LYP computations on the singlet PES.

Table 1
Quantum chemical parameters of all reacting species presented in this study at the B3LYP/LACVP* and M06/LACVP* level of theory in the gas phase.

Reactants	B3LYP/LACVP*				M06/LACVP*			
	μ (eV)	η (eV)	ω	ΔNmax	μ (eV)	η (eV)	ω	ΔNmax
TME	3.47	6.94	0.87	−0.50	3.69	7.38	0.92	−0.50
MnO_3Cl	−7.63	3.85	7.55	1.98	−7.73	4.36	6.85	1.77
TcO_3Cl	−7.31	5.07	5.27	1.44	−7.43	5.56	4.96	1.34
ReO_3Cl	−6.90	5.85	4.07	1.18	−7.04	6.50	3.81	1.08

Table 2
Rate constants (s^{-1}) for the formation of the various products in the oxidation of TME mediated by ReO_3Cl on the singlet PES in the gas phase.

ReO_3Cl	[3 + 2]	$[2 + 2]_a$	$[2 + 2]_b$	$[2 + 2]_c$
B3LYP	1.36×10^{-12}	2.44×10^{-19}	2.87×10^{-30}	4.12×10^{-26}
M06	6.49×10^{-9}	1.58×10^{-12}	1.58×10^{-22}	1.06×10^{-16}

Table 3
Rate constants (s^{-1}) for the formation of the various products in the oxidation of TME mediated by TcO_3Cl on the singlet PES in the gas phase.

TcO_3Cl	[3 + 2]	$[2 + 2]_a$	$[2 + 2]_b$	$[2 + 2]_c$	1X
B3LYP	2.60×10^{-1}	6.36×10^{-23}	3.22×10^{-15}	2.61×10^{-9}	1.10×10^{-6}
M06	1.77×10^{3}	7.19×10^{-14}	7.35×10^{-5}	$3.80 \times 10^{\circ}$	7.91×10^{-1}

Table 4
Rate constants (s^{-1}) for the formation of the various products in the oxidation of TME mediated by MnO_3Cl on the singlet PES in the gas phase.

MnO_3Cl	[2 + 1]	1X
B3LYP	6.15×10^{12}	1.83×10^{8}
M06	9.87×10^{11}	1.07×10^{12}

2.7. B3LYP results versus M06 results

From the theoretical results as discussed in the early result sections (all figures and tables), it is clear that the results (reaction energies, bond lengths, angles, and dipole moments) obtained from the M06 simulations are better than the B3LYP theoretical results on both singlet and triplet PESs.

The M06 functional is a global hybrid metageneralized gradient approximation (meta-GGA) with 27% of Hartree–Fock exchange, leading to a well-balanced functional for overall good performance for chemistry. For main group, organometallics, kinetics, and non-covalent bonds, M06 suite has a very good response under dispersion forces, improving one of the biggest deficiencies in DFT methods [7]. The s6 scaling factor on Grimme's long range dispersion correction is 0.25. This accounts for why M06/LACVP* simulations generally have slightly lower energies and shorter bond lengths compared to the B3LYP/LACVP.

3. Conclusion

The results from this theoretical study show that the [3 + 2] mechanistic pathway is both kinetically and thermodynamically favorable for the formation of diols for the oxidation of MO_3Cl (M = Tc and Re) by TME upon hydrolysis.

On the $MnMnO_3Cl$-catalyzedinglet PES, there are no side reactions that competed with the formation of the epoxides. Furthermore, for the MO_3Cl (M = Tc and Re) catalyzed surfaces, epoxide formation if plausible will form *via* the [2 + 2] mechanistic channel on the singlet PES, but not *via* the [3 + 2] or [2 + 1] direct pathway as evident from the DFT/B3LYP/LACVP* and DFT/M06/LACVP* computations. It was also observed that the reaction and activation energies computed at DFT/M06/LACVP* were lower compared to the DFT/B3LYP/LACVP* energies in all cases. From the computations, it is evident that MO_3Cl (M = Mn and Tc) is a good oxidation catalyst for olefinic substrates. Furthermore, frontier molecular orbital (FMO) analysis showed that the HOMO of the TME molecule couples with the LUMO of the MO_3Cl (Mn, Tc, and Re) complex on the singlet PES at both levels of theory. Also, it was observed that the dioxylation and epoxidation reaction mechanisms on the concerted reaction surface were stable over their formation on the stepwise reaction surface at all temperatures.

Moreover, from the quantum simulations, it can be predicted that the oxidation reaction at elevated temperatures tends to become more kinetically and thermodynamically unstable due to increasing free activation and reaction energies. Hence, the best condition to consider for the oxidation reaction studied will be at a temperature and pressure of 298.15 K and 1 atm respectively. Furthermore, the rate constant calculations suggested that the epoxidation process via the permanganyl chloride catalyzed surface was the fastest process of all catalyzed surfaces studied with the highest rate constant values at both levels of theories. Also, the [3 + 2] route was found to be faster than the competing [2 + 2] route in all cases on the singlet PES.

Conclusively, the theoretical results point out that the reaction mechanisms of the addition of TME to MO_3Cl complexes proceed similarly as seen in the oxidation of ethylene by MO_3Cl (M = Mn, Tc, and Re) complexes.

From the reactivity indices, the metal oxo complexes will act as the electrophiles whiles TME acts as the nucleophile with the permanganyl chloride being the best electrophile as observed from both levels of theories. It was also found that the electrophilic nature among the group VII B group decreases down the group, thus Mn > Tc > Re, which is in good correlation with the activation and reaction energies.

Ethical approval

Not applicable.

Authors' contributions

All authors (E.A.F, C.O, L.H, A.A, A.O, MKA, and A.M) have made a substantial, direct, and intellectual contribution to the work and approved it for publication.

Funding

We acknowledge The University of Ghana for financial support, The University of Johannesburg for using the Spartan cluster, and the Centre for High-Performance Computing (CHPC-South Africa) for using the cluster.

Availability of data and materials

Electronic supporting information data file is submitted. All data are included in this article and its supplementary material file.

Declaration of competing interest

The authors declare that they have no known competing financial interests or personal relationships that could have appeared to influence the work reported in this paper.

Data availability

Data will be made available on request.

Appendix A. Supplementary data

Supplementary data to this article can be found online at https://doi.org/10.1016/j.jmgm.2023.108419.

References

[1] M. Walker, A.J.A. Harvey, A. Sen, C.E.H. Dessent, Performance of M06, M06-2X, and M06-HF density functionals for conformationally flexible anionic clusters: M06 functionals perform better than B3LYP for a model system with dispersion and ionic hydrogen-bonding interactions, J. Phys. Chem. A 117 (47) (2013) 12590–12600, https://doi.org/10.1021/jp408166m.

[2] Y. Wang, P. Verma, X. Jin, D.G. Truhlar, X. He, Revised M06 density functional for main-group and transition-metal chemistry, Proc. Natl. Acad. Sci. U.S.A. 115 (41) (2018) 10257–10262, https://doi.org/10.1073/pnas.1810421115.

[3] A.D. Becke, Density-functional exchange-energy approximation with correct asymptotic behavior, Phys. Rev. A 38 (6) (1988) 3098–3100, https://doi.org/10.1103/PhysRevA.38.3098.

[4] A.D. Becke, A new dynamical correlation functional and implications for exact-exchange mixing, J. Chem. Phys. 104 (October 1995) 1040–1046, 1998.

[5] C. Lee, W. Yang, R.G. Parr, Development of the Colle-Salvetti correlation-energy formula into a functional of the electron density, Phys. Rev. B Condens. Matter 37 (2) (Jan. 1988) 785–789, https://doi.org/10.1103/physrevb.37.785.

[6] S.H. Vosko, L. Wilk, M. Nusair, Accurate spin-dependent electron liquid correlation energies for local spin density calculations: a critical analysis, Can. J. Phys. 58 (8) (1980) 1200–1211, https://doi.org/10.1139/p80-159.

[7] Y. Zhao, D.G. Truhlar, The M06 Suite of Density Functionals for Main Group Thermochemistry , Thermochemical Kinetics , Noncovalent Interactions , Excited States , and Transition Elements : Two New Functionals and Systematic Testing of Four M06-Class Functionals and 12 Other Fun, 2008, pp. 215–241, https://doi.org/10.1007/s00214-007-0310-x.

[8] R. Peverati, D.G. Truhlar, Quest for a universal density functional: the accuracy of density functionals across a broad spectrum of databases in chemistry and physics, Philos. Trans. R. Soc. A Math. Phys. Eng. Sci. 372 (2011) (2014), https://doi.org/10.1098/rsta.2012.0476.

[9] T. Sperger, I.A. Sanhueza, I. Kalvet, F. Schoenebeck, Computational studies of synthetically relevant homogeneous organometallic catalysis involving Ni, Pd, Ir, and Rh: an overview of commonly employed DFT methods and mechanistic insights, Chem. Rev. 115 (17) (2015) 9532–9586, https://doi.org/10.1021/acs.chemrev.5b00163.

[10] A. Aniagyei, R. Tia, E. Adei, A computational study of the addition of ReO3L (L = Cl−, CH3, OCH3 and Cp) to ethenone, SpringerPlus 5 (1) (2016), https://doi.org/10.1186/s40064-016-2012-0, 0–15.

[11] A. Dauth, J.A. Love, Reactivity by design-Metallaoxetanes as centerpieces in reaction development, Chem. Rev. 111 (3) (2011) 2010–2047, https://doi.org/10.1021/cr100388p.

[12] D.V. Deubel, Reactivity of osmium tetraoxide towards nitrogen heterocycles: implications for the molecular recognition of DNA mismatch, Angew. Chem. Int. Ed. 42 (17) (2003) 1974–1977, https://doi.org/10.1002/anie.200250462.

[13] M. Schröder, Osmium tetraoxide CIS hydroxylation of unsaturated substrates, Chem. Rev. 80 (2) (1980) 187–213, https://doi.org/10.1021/cr60324a003.

[14] H.C. Kolb, M.S. VanNieuwenhze, K.B. Sharpless, Catalytic asymmetric dihydroxylation, Chem. Rev. 94 (8) (1994) 2483–2547, https://doi.org/10.1021/cr00032a009.

[15] D.W. Nelson, et al., Toward an understanding of the high enantioselectivity in the osmium-catalyzed asymmetric dihydroxylation. 4. Electronic effects in amine-accelerated osmylations, J. Am. Chem. Soc. 119 (8) (1997) 1840–1858, https://doi.org/10.1021/ja961464t.

[16] R. Tia, E. Adei, [3+2] versus [2+2] addition of metal oxides across CC bonds: a theoretical study of the mechanisms of oxidation of ethylene by osmium oxide complexes, Comput. Theor. Chem. 977 (1–3) (2011) 140–147, https://doi.org/10.1016/j.comptc.2011.09.027.

[17] W.A. Herrmann, F.E. Kühn, Organorhenium oxides, Acc. Chem. Res. 30 (4) (1997) 169–180, https://doi.org/10.1021/ar9601398.

[18] W.A. Herrmann, P.W. Roesky, M. Wang, W. Scherer, Wolfgang A. Herrmann, * Peter W. Roesky, Mei Wang,$ and wolfgang scherer, Young 3 (9) (1994) 4531–4535.

[19] C.C. Romão, F.E. Kühn, W.A. Herrmann, Rhenium(VII) oxo and imido complexes: synthesis, structures, and applications, Chem. Rev. 97 (8) (1997) 3197–3246, https://doi.org/10.1021/cr9703212.

[20] R.M. Dickson, T. Ziegler, A density functional study of the electronic spectrum of permanganate, Int. J. Quant. Chem. 58 (6) (1996) 681–687, https://doi.org/10.1002/(SICI)1097-461X(1996)58:6<681::AID-QUA10>3.0.CO;2-0.

[21] W.A. Herrmann, R. Alberto, P. Kiprof, F. Baumgärtner, Alkyltechnetium oxides: first examples and reactions, Angew Chem. Int. Ed. Engl. 29 (2) (1990) 189–191, https://doi.org/10.1002/anie.199001891.

[22] E.A. Fosu, C. Obuah, L. Hamenu, A. Aniagyei, M.K. Ainooson, K.K. Govender, Quantum mechanistic studies of the oxidation of ethylene by rhenium oxo complexes, J. Chem. 2021 (2021), 7931956, https://doi.org/10.1155/2021/7931956.

[23] D.V. Deubel, G. Frenking, [3+2] versus [2+2] addition of metal oxides across C=C bonds. Reconciliation of experiment and theory, Acc. Chem. Res. 36 (9) (2003) 645–651, https://doi.org/10.1021/ar020268q.

[24] T. Wistuba, C. Limberg, The reaction of permanganyl chloride with olefins: intermediates and mechanism as derived from matrix-isolation studies and density functional theory calculations, Chem. Eur J. 7 (21) (2001) 4674–4685, https://doi.org/10.1002/1521-3765(20011105)7:21<4674::AID-CHEM4674>3.0.CO;2-L.

[25] A. Aniagyei, C. Kwawu, R. Tia, E. Adei, Permanganyl chloride-mediated oxidation of tetramethylethylene: a density functional theory study, J. Mol. Graph. Model. 98 (2020), 107616, https://doi.org/10.1016/j.jmgm.2020.107616.

[26] F.J. Devlin, J.W. Finley, P.J. Stephens, M.J. Frisch, Ab Initio calculation of vibrational absorption and circular dichroism spectra using density functional force fields: a comparison of local, nonlocal, and hybrid density functionals, J. Phys. Chem. 99 (46) (Nov. 1995) 16883–16902, https://doi.org/10.1021/j100046a014.

[27] W. Hehre, S. Ohlinger, P. Klunzinger, B. Deppmeier, A. Driessen, J. Johnson, Spartan'16 Tutorial and User's Guide, 2017, p. 552.

[28] Development of the Colic-Salvetti correlation-energy into a functional of the electron density formula, J. Chem. Phys. 98 (2) (1993) 1372–1377, https://doi.org/10.1063/1.464304.

[29] M. Clark, R.D. Cramer, N. Van Opdenbosch, Validation of the general purpose tripos 5.2 force field, J. Comput. Chem. 10 (8) (1989) 982–1012, https://doi.org/10.1002/jcc.540100804.

[30] K.B. Sharpless, A.Y. Teranishi, J.E. Bäckvall, Chromyl chloride oxidations of olefins. Possible role of organometallic intermediates in the oxidations of olefins by oxo transition metal species, J. Am. Chem. Soc. 99 (9) (1977) 3120–3128, https://doi.org/10.1021/ja00451a043.

[31] E.A. Fosu, et al., A DFT study on the reaction mechanisms of the oxidation of ethylene mediated by technetium and manganese oxo complexes, J. Mol. Model. 28 (4) (2022) 94, https://doi.org/10.1007/s00894-022-05092-0.

[32] L.R. Domingo, M.J. Aurell, P. Pérez, R. Contreras, Quantitative characterization of the local electrophilicity of organic molecules. Understanding the regioselectivity on Diels−Alder reactions, J. Phys. Chem. A 106 (29) (Jul. 2002) 6871–6875, https://doi.org/10.1021/jp020715j.

[33] R.G. Parr, L.v. Szentpály, S. Liu, Electrophilicity index, J. Am. Chem. Soc. 121 (9) (Mar. 1999) 1922–1924, https://doi.org/10.1021/ja983494x.

[34] T. Koopmans, Über die Zuordnung von Wellenfunktionen und Eigenwerten zu den Einzelnen Elektronen Eines Atoms, Physica 1 (1) (1934) 104–113, https://doi.org/10.1016/S0031-8914(34)90011-2.

[35] M.M. Efremova, A.S. Novikov, R.R. Kostikov, T.L. Panikorovsky, A. V Ivanov, A. P. Molchanov, Regio- and diastereoselectivity of the cycloaddition of nitrones with N-propadienylindole and pyrroles, Tetrahedron 74 (1) (2018) 174–183, https://doi.org/10.1016/j.tet.2017.11.056.

[36] J.P. Ranck, Modern physical chemistry: a molecular approach (duffey, george H.), J. Chem. Educ. 78 (8) (Aug. 2001) 1024, https://doi.org/10.1021/ed078p1024.